

All-dielectric nanophotonics: the quest for better materials and fabrication techniques

Denis G. Baranov^{†,1,2,*} Dmitry A. Zuev^{†,3} Sergey I. Lepeshov,³ Oleg V. Kotov,⁴
Alexander E. Krasnok,⁵ Andrey B. Evlyukhin,^{6,3} and Boris N. Chichkov^{6,7}

¹*Moscow Institute of Physics and Technology, 9 Institutskiy per., Dolgoprudny 141700, Russia*

²*Department of Physics, Chalmers University of Technology, 412 96 Gothenburg, Sweden*

³*ITMO University, Saint Petersburg, Russia*

⁴*N. L. Dukhov Research Institute of Automatics, Moscow 127055, Russia*

⁵*Department of Electrical and Computer Engineering,
The University of Texas at Austin, Austin, Texas 78712, USA*

⁶*Laser Zentrum Hannover e.V, Hannover, Germany*

⁷*Leibniz Universität, Hannover, Germany*

All-dielectric nanophotonics is an exciting and rapidly developing area of nanooptics which utilizes the resonant behavior of high-index low-loss dielectric nanoparticles for enhancing light-matter interaction on the nanoscale. When experimental implementation of a specific all-dielectric nanostructure is an issue, two crucial factors have to be in focus: the choice of a high-index material and a fabrication method. The degree to which various effects can be enhanced relies on the dielectric response of the chosen material as well as the fabrication accuracy. Here, we make an overview of available high-index materials and existing fabrication techniques for the realization of all-dielectric nanostructures. We compare performance of the chosen materials in the visible and IR spectral ranges in terms of scattering efficiencies and Q -factors. Various fabrication methods of all-dielectric nanostructures are further discussed, and their advantages and disadvantages are highlighted. We also present an outlook for the search of better materials with higher refractive indices and novel fabrication methods enabling low-cost manufacturing of optically resonant high-index nanoparticles. We hope that our results will be valuable for researches across the whole field of nanophotonics and particularly for the design of all-dielectric nanostructures.

INTRODUCTION

Plasmonics, the study of extraordinary optical properties of metallic nanoparticles, has been the avant-garde of nanophotonics for more than a decade. The intense research in this field has arisen due to the ability of nanoparticles made of noble metals (gold, silver) to enhance the electromagnetic field on the nanoscale enabling the unprecedented opportunities for boosting various optical effects and manipulation of electromagnetic radiation in unusual ways [1–4]. However, high level of Joule losses associated with the free electron response of noble metals was always a challenge limiting the efficiency of optical devices [5–7]. Although certain loss compensation approaches for plasmonic nanostructures based on gain media [8–13] and very special configuration of the metal conduction band [14] have been suggested, their versatile implementation has proven to be challenging. As a result, the problem of Joule damping has motivated researches to search for alternatives to noble metals, such as heavily doped semiconductors [15] and polar crystals exhibiting Reststrahlen bands [16].

Mie resonances of *high-index dielectric nanoparticles* pave an alternative route towards the development of nanostructures with special optical properties. Although Mie theory, which predicts the resonant behavior of high-index subwavelength particles, exists for more than a century [17], the enormous interest in optical properties of all-dielectric nanostructures has arisen only recently with observation of low-order Mie modes in sil-

icon colloids [18, 19] and thanks to the advances in fabrication of single dielectric nanoparticles with controlled geometry [20–24]. Resonant behavior of high-index nanoparticles not only enables realization of low-loss non-plasmonic metamaterials and metasurfaces [25–28] with rich optical functionalities [29–34], but also pave the way to enhanced light-matter interaction [35–38] as well as advanced linear [39–47] and nonlinear [48–51] light manipulation.

All-dielectric nanophotonics offers a variety of intriguing optical effects and enables promising practical applications. In order to implement these possibilities, *materials with specific optical properties* are desired, and certain *fabrication methods* must be available. Although the technologies of manufacturing of silicon particles are well established today, silicon is not the only candidate for high-index Mie resonators. There is a plethora of semiconductors and polar materials exhibiting attractive characteristics in visible and IR spectral regions in the context of all-dielectric nanophotonics. Here, we present a comparative analysis of available high-index materials in view of their performance as optical nanoresonators. The resonant behavior is analyzed in terms of linear characteristics of spherical nanoparticles. To complement this analysis, we review the existing fabrication methods of nanostructures from various high-index materials. Finally, we provide motivations for the search of better materials with higher refractive index and novel fabrication methods enabling low-cost manufacturing of optically resonant dielectric nanoparticles.

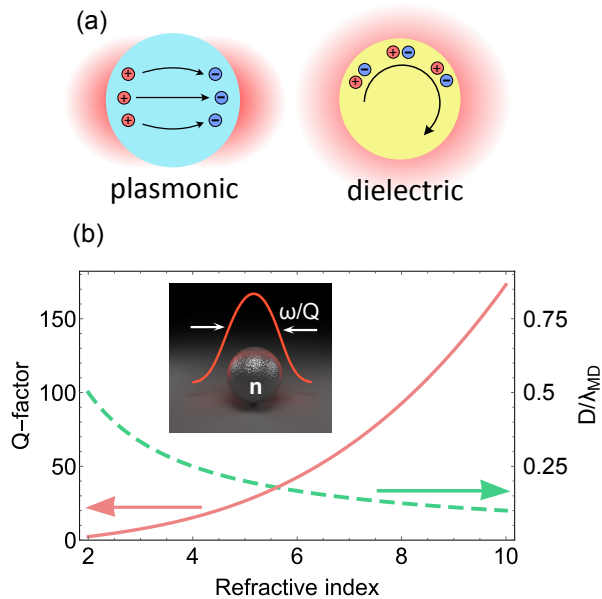


FIG. 1. (a) Schematic illustration of fundamental resonances and induced currents in plasmonic and dielectric nanoparticles. Free electrons of the metal give rise to the conduction currents in plasmonic nanoparticles, while bounded charges in dielectrics cannot move freely across the particle and give rise to the displacement currents. (b) Refractive index dependence of the Q -factor of the magnetic dipole resonance of a spherical nanoparticle and the respective dependence of the resonant nanoparticle diameter D . The nanoparticle size is continuously tuned such that it satisfies the MD resonance condition at each point.

OVERVIEW OF HIGH-INDEX MATERIALS

Basics of light scattering

To set the stage, let us recall the basics of light scattering by spherical particles. Electromagnetic response of a spherical particle made of material with permittivity ϵ of any size is exactly described by Mie theory [17]. In this framework, the electromagnetic field scattered by a sphere is represented as a sum of electric-type (TM) and magnetic-type (TE) spherical harmonics. Amplitudes of these harmonics are described by the Mie coefficients a_n for the electric modes and b_n for the magnetic modes. Each of these amplitudes has a set of resonance frequencies, at which electromagnetic field of the corresponding harmonic is enhanced both inside and outside of the sphere.

Enhancement of optical phenomena by resonant nanostructures can be described with various figures of merit. In the context of spectroscopic applications the local electric field enhancement is the crucial parameter which defines the efficiency of such processes as spontaneous emission, Raman scattering, higher harmonics generation and others [52–54]. Using the temporal coupled mode theory,

the local field enhancement (averaged over the mode volume) may be expressed as follows [55]:

$$\left(\frac{E_{\text{loc}}}{E_{\text{inc}}}\right)^2 \propto \gamma_{\text{rad}} \frac{Q^2}{V}, \quad (1)$$

where γ_{rad} is the nanoantenna radiative damping rate, Q is the quality factor of the excited mode, V is its mode volume. Expression (1) suggests that high Q and small V are beneficial for the local field enhancement with nanoantennas.

In contrast to plasmonics, where the Joule losses represent the dominant dissipation channel, the Q -factor of high-index Mie resonators is mainly limited by the radiation damping. In the context of metasurfaces, which manipulate the characteristics of propagating fields, radiation should not be treated as a loss. For this reason, a relevant figure of merit is the nanoantenna radiation efficiency η_{rad} :

$$\eta_{\text{rad}} = \frac{\sigma_{\text{scat}}}{\sigma_{\text{scat}} + \sigma_{\text{abs}}} \quad (2)$$

with σ_{scat} and σ_{abs} being the scattering and absorption cross-sections, respectively. Value of η_{rad} close to 1 indicates that almost all incident light is re-radiated without being absorbed by nanoantennas constituting a metasurface. At the same time, a smaller nanoantenna size is also desired since it would allow smaller distances between neighboring nanoantennas reducing the spatial dispersion effect.

The extraordinary enhancement of electric field by metallic nanoparticles relies on free electron response, Fig. 1(a). When the frequency of incident light matches that of the free electron oscillations inside a sphere, strong electric field is produced in the vicinity of the particle. These oscillations, however, are accompanied by significant optical loss arising from both intraband and interband transitions and eventually lead to heating of the resonator [7]. In contrast, optical resonances of high-index nanoparticles originate from the *displacement currents* due to oscillations of bounded electrons, Fig. 1(a). These currents are free of Ohmic damping, what allows to reduce non-radiative losses and heating of an optical cavity.

Of special interest to the field of nanophotonics is the *magnetic dipole (MD) resonance* of high-index nanoparticles - the fundamental magnetic dipolar mode of a dielectric sphere. At a fixed nanosphere diameter, the MD resonance occurs at the smallest frequency of the incident wave compared to other resonances [20, 29]. Under the resonance condition, electric fields are anti-parallel at the opposite boundaries of the sphere, which gives rise to strong coupling to circulating displacement currents characteristic for a magnetic dipole mode [22].

The spectral position of the MD resonance of a spherical particle is approximately defined by $\lambda_{\text{MD}} \approx nD$ with

n being the refractive index of the sphere and D its diameter. Therefore, larger refractive indices are desirable from the point of view of device miniaturization. The field enhancement and Q -factor of Mie resonances also benefit from the large particle refractive index (see Fig. 1(b)) – this may be intuitively understood as the result of smaller radiation leakage from nanoparticles with larger refractive index contrast.

High refractive index materials

The above considerations clearly pose the *quest for materials* with large refractive indices. In the visible and near-IR spectral ranges, the highest known permittivities are demonstrated by semiconductors such as Si, Ge, GaSb and others, see Fig. 2(a). In the neighboring mid-IR range, which is also of great interest to the optoelectronic technology, narrow-band semiconductors and polar crystals demonstrate very attractive characteristics, and have been implemented for the design of all-dielectric metamaterials consisting of resonant Te [28] and SiC [27] elements.

The origin of relatively high refractive index of these materials can be understood from the picture of their electronic response, see Fig. 2(b). While in the low frequency regime the response is purely dielectric (assuming that we are dealing with undoped materials), in the visible and IR spectral ranges these materials exhibit a series of resonances. Due to the coupling of light to these resonances of the medium, the regions of increased refractive index appear in the spectrum. The low frequency phonon-polariton resonance occurs due to coupling of light with optical phonons of the crystal lattice of polar crystals [56, 57]. The higher frequency exciton-polariton resonance originates from interband transitions in semiconductors and forms a pronounced plateau in their dielectric function.

The high refractive index of these materials comes at a cost of increased absorption. According to the Kramers-Kronig relations [58], any dispersion of permittivity is related to dissipation. As it was pointed above, the high-index regions of semiconductors and polar crystals stem from their exciton and phonon resonances which bring optical absorption. This fundamental trade-off between absorption and high refractive index eventually sets the limit to all-dielectric resonator performance.

There is a significant difference between the behavior of refractive indices of semiconductors and polar crystals. In semiconductors, the high refractive index at below-band gap frequencies originates from a continuum of interband transitions [57], what allows one to have high index and relatively low absorption at the same time. In polar crystals, high index is related to a single phonon resonance, so that it is accompanied by large absorption coefficient [59].

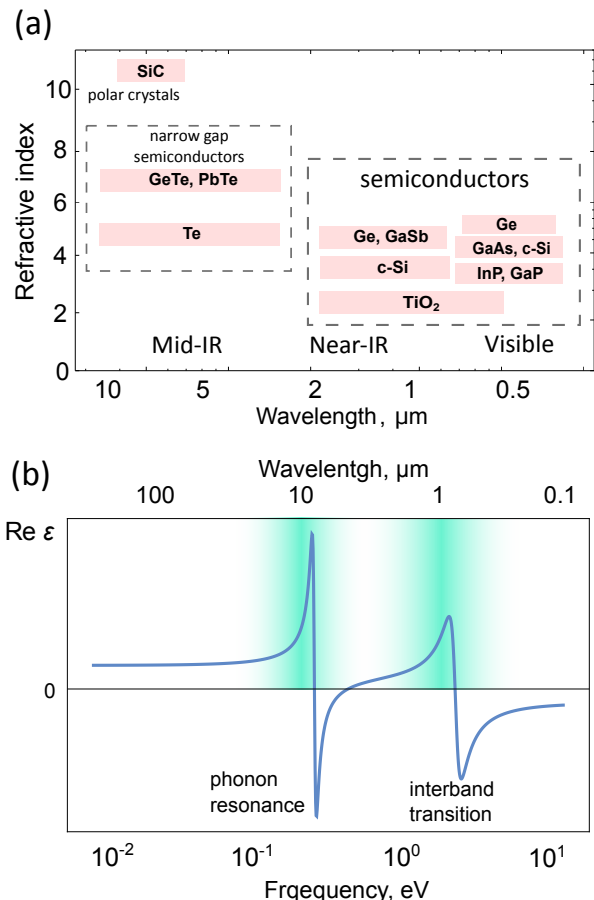


FIG. 2. (a) Refractive indices of materials available for dielectric nanophotonics from visible to mid-IR spectral ranges. (b) A typical dielectric response of a high-index material exhibiting a series of resonances. Shaded area depicts two high-index plateau related to material resonances.

The value of refractive index of a semiconductor is closely related to its electronic band gap. Generally, the *electrostatic* refractive index of a semiconductor decreases with the increasing energy gap. This correlation can be understood from the following argument, suggested by Moss [72]. He considered electrons in semiconductor as if they were bound to a Hydrogen atom. The energy needed to ionize the atom and to raise an electron to the conduction band scales as $E_g \sim 1/\epsilon^2$, where ϵ is the background permittivity of the semiconductor. This results in a very simple approximation for the static refractive index known as the Moss formula:

$$n^4 E_g = 95 \text{ eV}. \quad (3)$$

There are several other models leading to similar dependencies [73, 74]. Although being valid for static permittivity, this approximation qualitatively reproduces behavior of refractive indices at optical and IR wavelengths, summarized in Fig. 2(a): overall, narrow gap semiconductors such as PbTe, GeTe demonstrate higher refrac-

| Material | Spectral range, μm | Refractive index, n | Extinction coefficient, k | Bandgap type | Bandgap energy, eV | Reference |
|------------------|-------------------------|-----------------------|-----------------------------|--------------|--------------------|-----------|
| c-Si | 0.50 – 1.45 | 4.293 – 3.486 | 0.045 – 0.001 | indirect | 1.12 | 60 |
| | 1.45 – 2.40 | 3.484 – 3.437 | ~ 0 | | | 61 |
| a-Si | 0.50 – 1.00 | 4.47 – 3.61 | 1.12 – 0.01 | indirect | 1.50 | 62 |
| GaAs | 0.50 – 0.80 | 4.037 – 3.679 | 0.376 – 0.089 | direct | 1.46 | 63 |
| GaP | 0.50 – 0.80 | 3.590 – 3.197 | ~ 0 | indirect | 2.26 | 63 |
| InP | 0.50 – 0.80 | 3.456 – 3.818 | 0.203 – 0.511 | direct | 1.27 | 64 |
| TiO ₂ | 0.50 – 1.00 | 2.715 – 2.483 | ~ 0 | indirect | 3.05 | 65 |
| Ge | 0.50 – 0.60 | 4.460 – 5.811 | 2.366 – 1.389 | indirect | 0.67 | 63 |
| | 0.60 – 0.80 | 5.811 – 4.699 | 1.389 – 0.3 | | | 66 |
| | 0.80 – 1.90 | 4.684 – 4.129 | 0.3 – 0.001 | | | 61 |
| | 1.90 – 2.40 | 4.111 – 4.069 | ~ 0 | | | |
| GaSb | 1.00 – 2.40 | 4.140 – 3.846 | 0.225 – 0.001 | direct | 0.69 | 67 |
| Te | 4.00 – 14.0 | 4.929 – 4.785 | ~ 0 | indirect | 0.34 | 68 |
| PbTe | 4.10 – 12.5 | 5.975 – 5.609 | ~ 0 | direct | 0.31 | 69 |
| GeTe | 6.20 – 11.8 | 7.3 – 7.278 | ~ 0 | direct | 0.2 | 70 |
| SiC | 11.0 – 15.0 | ~ 20 | ~ 15 | - | - | 71 |

TABLE I. Optical properties of high index materials.

tive indices than those with energy gap lying in the visible. The detailed information on optical properties of chosen materials including values of the extinction coefficients and electronic band gap as well as the sources from which the data on permittivity dispersion is presented in Table I.

Semiconductor materials may have either direct or indirect band gap, what has a profound implication on the absorbing properties. When light passes through a direct bandgap semiconductor, a photon can be absorbed to the conduction band. At the same time, when light travels through an indirect band gap medium, due to large mismatch between the electron and photon wavevectors, such process does not occur what results in reduced optical absorption. Nevertheless, even direct band gap materials may demonstrate good performance if the operation frequency lies below the band gap, such as the case of GaSb in the mid-IR range (see below).

Comparative analysis of materials

Let us now illustrate performance of the available high-index materials for the case of a spherical particle since it allows exact analytical solution. First, we present in Figs. 3(a)–(c) the Q -factor of the MD resonance of a spherical particle as a function of wavelength. In order to obtain this dependence, we continuously tune the nanoparticle size such that it satisfies the MD resonance

condition at each wavelength. The Q -factor was obtained by calculating the full-width of the MD resonance scattering cross-section. The results show that across the whole visible spectral range among all semiconductors, c-Si demonstrates the highest Q -factor of around 13 with the closest being GaP with Q -factor of only around 10. Good performance of c-Si and GaP is caused by the fact that these two materials are indirect band gap semiconductors, what results in the reduced optical absorption and therefore higher Q -factors. In the near-IR, Ge takes the pedestal with Q -factor slightly above 15 at the most interesting wavelength of 1.55 μm . Notably, GaSb demonstrates good values of the Q -factor at wavelengths above 1.8 μm despite being a direct semiconductor. In the mid-IR, the situation is strikingly different: particles of narrow band gap semiconductors PbTe and GeTe demonstrate Q -factor well above 40 and 70, respectively. SiC, on the other hand, despite its huge refractive index exceeding 10, shows very low quality factor. Such poor optical response of SiC nanoparticles stems from narrow phonon resonance of the polar crystal associated with large absorption, as argued above.

The results presented in Figs. 3(d)–(f) indicate that the radiation efficiencies of semiconductor nanoparticles η_{rad} calculated with Eq. 2 generally increase with the increasing wavelength. Interestingly, in the visible range the highest radiation efficiency is demonstrated by TiO₂ and GaP nanoparticles due to the widest electronic bandgap and thus the smallest absorption among the studied ma-

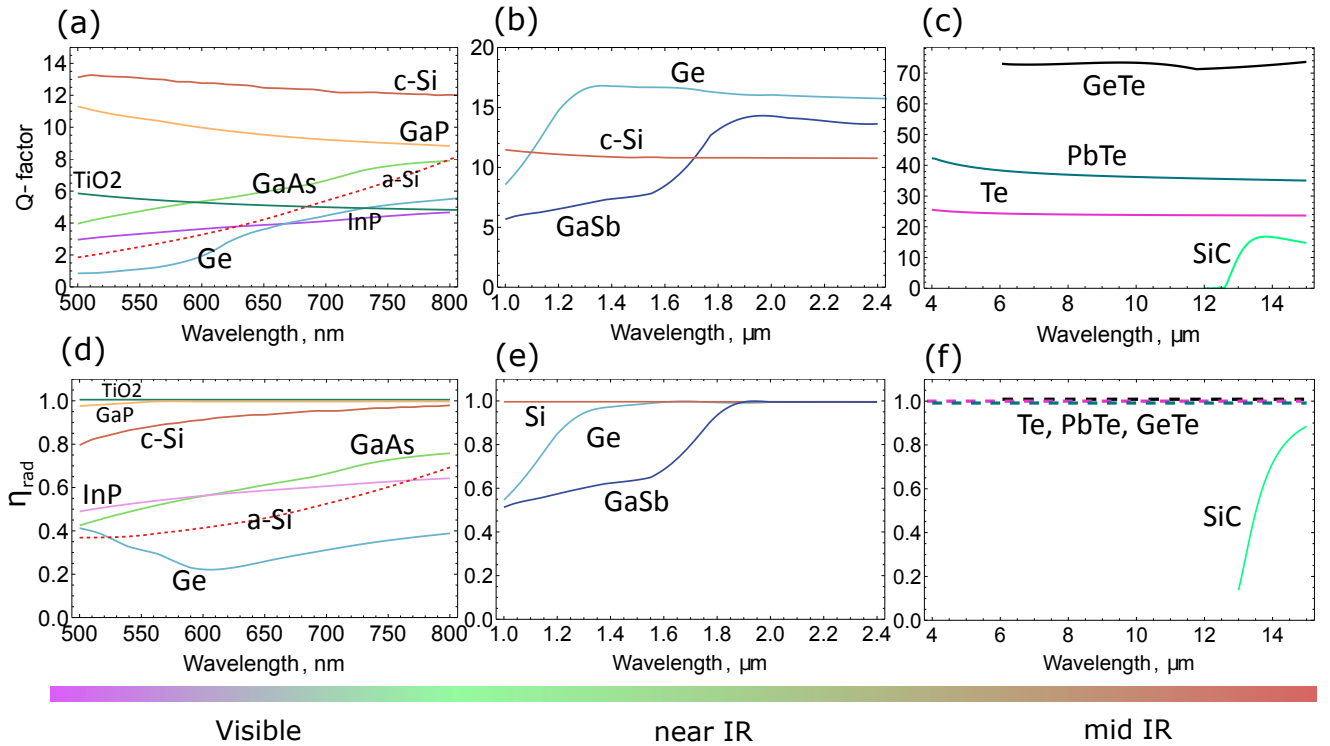


FIG. 3. Quantitative comparison of the available high-index materials for all-dielectric nanophotonics. (a)–(c) Q -factors of the magnetic dipole (MD) resonance of spherical nanoparticles made of various high-index materials as a function of wavelength in the visible (a), near-IR (b) and mid-IR (c) regions. (d)–(f) The antenna radiation efficiency η_{rad} at the MD resonance for the same scope of materials.

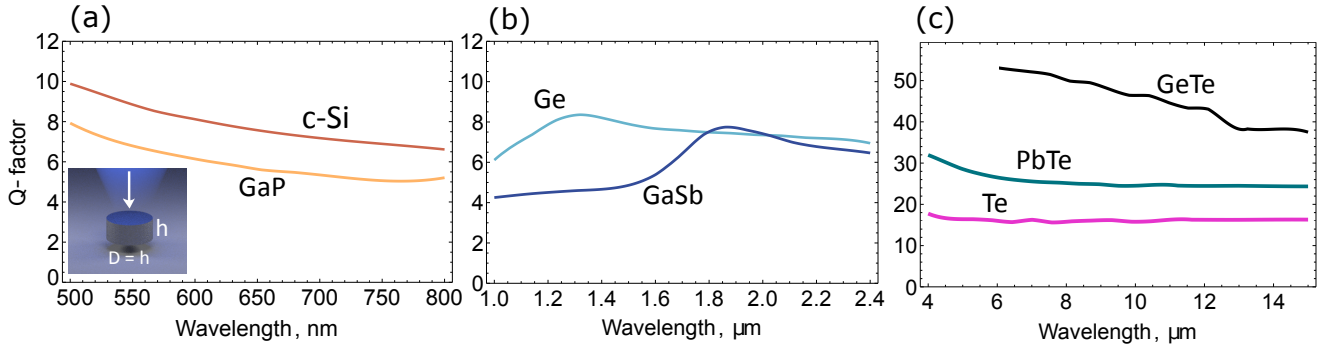


FIG. 4. Q -factors of the MD resonance of nanodisks with equal height and diameter. The nanodisk sizes were continuously tuned such that it satisfies the MD resonance condition at each wavelength.

materials, see Table I. In the near-IR, the efficiency of Ge and Si antennas is nearly one at wavelengths longer than $1.5 \mu\text{m}$. In the mid-IR, the efficiencies of Te, PbTe and GeTe particles are equal to 1, while SiC particles show very poor performance with low radiation efficiency and Q -factor owing to the sharp phonon resonance.

Although the spherical geometry of a particle is attractive from the theoretical standpoint, as it allows exact analytical description of light scattering, fabrication of spherical particles is not always an option. On the other hand, Mie resonances occur for a wide range of particle shapes, including nanodisks which may be easily fabri-

cated by the standard nanolithography techniques (see Section III A) for any material considered in this study. For this reason, we performed the same analysis of Q -factors for nanodisks made of different materials. The results shown in Fig. 4 demonstrate that behavior of Q -factors is overall similar to that observed for spherical particles. To conclude this section, we finally note that the observed Q -factor values do not set the upper limit for high-index nanostructures, and larger Q -factors can be obtained in clusters of nanoparticles, such as dimers and metasurfaces [32, 75, 76].

OVERVIEW OF FABRICATION TECHNIQUES

Bearing in mind the above considerations about high-index materials, we now may proceed to a brief review of the existing fabrication techniques. The rapid progress of nanotechnology has enabled tremendous development of methods for semiconductor nanoparticle fabrication. The most illustrative example is presented by silicon, since it is the most frequently used high-index material in the visible and IR ranges owing to its relatively low cost and low imaginary part of the refractive index. Therefore, it is not surprising, that methods of fabrication of silicon nanostructures have been first historically developed. Initially, different methods for fabrication of optically small and non-resonant silicon nanoparticles were developed basically for biological imaging and drug delivery (Ref. 97), including methods of mechanical milling [98], pulsed laser ablation in liquid [99], electrochemical etching [100], gas phase synthesis [101], etc.

In the context of nanophotonic applications, nanoparticles with the magnetic and electric resonances located in the visible or near-infrared spectral regions are desired. This requirement sets up high demands not only to the nanoparticle size, but also to repeatability and throughput of fabrication methods, precise control of nanoparticle geometry, simplicity of the fabrication procedure (quantity of steps involved in the fabrication process), and manipulation of nanoparticle space arrangement. Therefore, the development of fabrication technologies of Mie-resonant high-index nanoparticles has recently been initiated, that resulted in emergence of various techniques, roughly summarized in four groups in the Table II. This table demonstrates that all techniques have inherent advantages and disadvantages. Thus, the choice of a fabrication method of high-index nanoparticles is determined by the objectives of the investigation, e.g. in case of high demands to chemical purity, laser-assisted methods are preferable, in contrast, if high-productivity is a cornerstone, chemical methods will be considered as more preferable ones. To better understand applicability of these methods for a special case, they should be carefully considered on the example of fabricated high-index nanostructures.

Lithography

Single nanostructures

The most straightforward methods for fabrication of nanostructures involve lithography, since it provides high repeatability alongside with an opportunity to fabricate nanostructures of complicated shapes via combination of lithographic processes. The conventional lithographic methods have been successfully applied for the fabrication of single nanostructures. For example, silicon

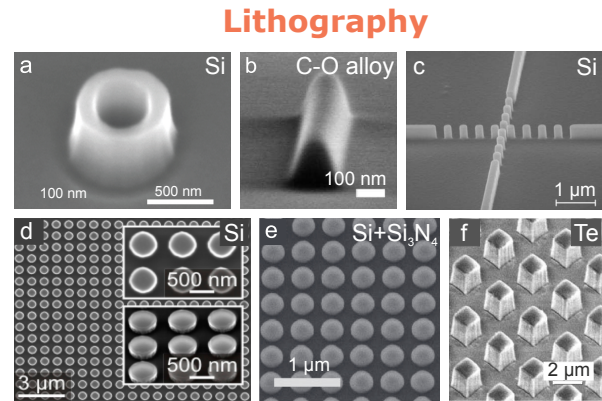


FIG. 5. (a) Scanning electron microscopy (SEM) image of hollow Si cylinder. Reprinted with permission from Ref. 78. (b) SEM image of carbonaceous dielectric nanorod antenna fabricated by electron beam-induced deposition. Reprinted with permission from Ref. 79. (c) Periodic dielectric waveguide crossing. Reprinted with permission from Ref. 80. (d) Silicon nanoparticles obtained by means of reactive-ion-etching through a mask. Reprinted with permission from Ref. 81. (e) Si nanoparticles with additionally deposited Si_3N_4 thin film, reprinted with permission from Ref. 82. (f) High-index cubic tellurium resonators, reprinted with permission from Ref. 28

nanoresonators consisting of hollow nanocylinders with an outer diameter of 108–251 nm and a gap size >20 nm were fabricated by the combination of electron beam lithography with reactive ion etching, Fig. 5(a) [78]. The geometry of these structures (the outer diameter, height and wall thickness) can be varied to control the resonant wavelength and relative spectral spacing of the modes.

In Ref. 79, a single dielectric nano-rod antenna (see Fig. 5(b)) consisted of amorphous alloys of C and O was fabricated via electron beam-induced deposition. The control of nanoantenna geometry via fabrication process was applied for resonant light scattering control over the whole visible wavelength range. In Ref. 80, the intersection region of two silicon waveguides was replaced by an array of silicon cylinders, Fig. 5(c). The proposed method of high-index nanostructure fabrication is very promising for optical cross connects because the cylinder structure is compatible with the existing lithography processes, can be fabricated synchronously with waveguide components as well as demonstrates high transmission and negligible cross talk over a broad bandwidth.

Nanostructure arrays

The standard micro/nanofabrication processing techniques are proven to be effective means of fabrication of large scale nanostructure arrays. The fabrication of large-scale arrays is very important for the creation of high-index metasurfaces setting higher demands to the

| Method | Advantages | Disadvantages |
|---|---|---|
| Lithography [18, 77–86] | <ul style="list-style-type: none"> - high resolution (below 10 nm) - high repeatability - complicated nanostructures can be fabricated | <ul style="list-style-type: none"> - non-single step process - spherical shape is not accessible in nanolithography methods - complicated equipment |
| Thermal dewetting [87–90] | <ul style="list-style-type: none"> - high-productivity - simplicity | <ul style="list-style-type: none"> - precision control of size and location of the nanoparticles can be achieved only via additional methods |
| Chemical methods [27, 91–93] | <ul style="list-style-type: none"> - high-productivity - nanoparticles can be fabricated in colloid immediately | <ul style="list-style-type: none"> - chemical waste - necessity of nanoparticles additional ordering - contamination of nanoparticles during fabrication is possible |
| Laser-assisted methods [20–22, 44, 75, 94–96] | <ul style="list-style-type: none"> - single step process - simplicity - high repeatability - lack of harmful chemical waste - amorphous or crystalline nanoparticles can be produced | <ul style="list-style-type: none"> - need in a film preparation for the process - high reliability of the mechanic systems in experimental setup - high demands to focusing and laser beam shape |

TABLE II. Summary of the available methods for fabrication of all-dielectric nanostructures.

precision and reproducibility of nanostructures. The controllable fabrication of silicon nanoparticle arrays was achieved by a multi-step method, including electron-beam lithography on silicon-on-insulator wafers (formation of mask from resist) and reactive-ion-etching process with following removal of remaining electron-beam resist mask. This technology allows forming arrays of silicon nanodisks, Fig. 5(d) [81], in which Mie-resonances can be precisely tuned by varying basic geometrical parameters (diameter and height). More complicated nanostructures representing the combination of Si nanoparticles, produced on the silicon wafers by substrate conformal soft-imprint lithography in combination with reactive ion etching, and a Si_3N_4 coating, Ref. 82 (see Fig. 5(e)) are demonstrated for the average reflectivity reduction up to the values lower than 3% over the wide spectral range of 450–900 nm.

Multi-step lithography methods have been also implemented for the fabrication of high-index tellurium dielectric resonators for all-dielectric metamaterial, see Fig. 5(f) [28]. For these experiments, BaF_2 optical flat substrate was applied for deposition of $1.7 \mu\text{m}$ Te thick film by electron-beam evaporation. Then, this film was patterned using electron-beam lithography and a reactive ion etching process to fabricate uniform structure. Zero backscattering and significant light dispersion in forward direction were demonstrated in GaAs nanoparticles, fabricated with molecular beam epitaxy, lift-off

procedure, reactive ion and plasma etching [83]. The Te dielectric metamaterial structure was also made in Ref. 84 using multi-cycle deposition-etching-lift-off technique. In Ref. 85, an array of TiO_2 nanostructures on a Al_2O_3 -passivated Si wafer was produced by a combination of standard lithography methods: substrate-conformal imprint lithography, reactive ion etching and plasma assisted atomic layer deposition (ALD). These procedures made possible fabrication of nano-patterned dielectric coating for crystalline Si solar cells possessing anti-reflection properties due to preferential forward scattering of light via proper engineering of Mie resonances of TiO_2 nanocylinders. The combination of e-beam lithography and dielectric reactive ion etching was also successfully implemented to metasurface demonstrating Q-factor of 350 (for Si-based structure) and Q-factor of 600 (for GaAs-based structure) in the near-infrared ($1 \mu\text{m}$) [76]

Another approach to fabrication of planar optical metasurfaces based on high-quality TiO_2 grown by ALD has been demonstrated in Refs. 33, 102 (see also Ref. 103 for a review of planar optical metasurfaces). Here, ALD provides precise control of film thickness (up to a monolayer) and the material phase, making possible creation of high aspect-ratio nanostructures with no losses in the visible region. The proposed approach can be applied to any type of metasurfaces.

Thus, lithographic methods remain more reliable for

high-index nanostructure fabrication combining three important qualities: high reproducibility for the nanostructure arrays, possibility of fabrication of nanostructures with complex shape, and high resolution. More information on lithographic fabrication of dielectric nanostructures can be found in Ref. 86. It should be mentioned, that in spite of these advantages, the methods can hardly be applied for the creation of spherical nanoparticles that represent interest not only for fundamental but also for applied sciences. Moreover, multiple steps, that are often required for high-index nanostructure fabrication, as well as, complexity and high cost of equipment motivate researchers to look for novel fabrication methods.

Chemical methods

Chemical methods are promising in terms of high-throughput fabrication of nanoparticles. These methods also offer flexibility in synthesis of materials, relative simplicity, and compatibility with other methods of solid material synthesis. One of the most widespread methods is the chemical vapor deposition technique. This process can be applied as an effective method for the fabrication of silicon nanoparticles with different sizes: e.g. fabrication of silicon nanoparticles can be carried out by decomposition of disilane gas (Si_2H_6) at high temperatures into solid silicon and hydrogen by the following chemical reaction: $\text{Si}_2\text{H}_6 \rightarrow 2\text{Si(s)} + 3\text{H}_2\text{(g)}$. As a result, spherical polydisperse silicon particles with diameters from 0.5 to 5 μm (Ref. 18) and about 300 – 500 nm (Ref. 77) were produced by this method. The decomposition temperature of the precursor as well as annealing treatment can be chosen to fabricate amorphous or polycrystalline particles with a crystallite size of about 3 nm. It is interesting, that appearance of unwanted silicon dust in the decomposition of silicon precursors is mentioned in Ref. 104. In fact, this dust is composed of silicon nano and microspheres, as it is demonstrated in Refs. 18, 77.

The crystalline silicon Mie resonators can be also created via alkaline chemical etching combined with electronic lithography [91]. This method eliminates reactive ion etching and can be applied for the fabrication of both silicon nanoresonators and oligomers. Further, fabrication of a monodispersed silicon colloid was achieved via decomposition of trisilane (Si_3H_8) in supercritical n-hexane at high temperature [92]. In this method, the particles size can be controlled by changing the trisilane concentration and reaction temperature. With this method a plenty of similar silicon nanoparticles with size dispersion in the range of several percents, which can be ordered into hexagonal lattice by self-assembly, Fig. 6(a), can be obtained. The main disadvantage of this method is the porosity and high hydrogen content of nanoparticles, as well as, the necessity of additional patterning

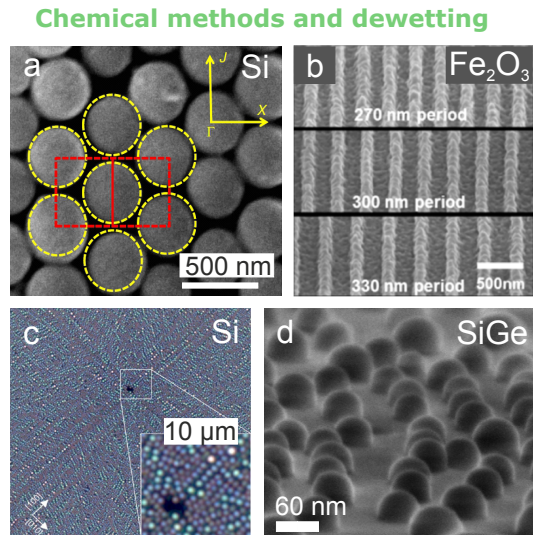


FIG. 6. (a) self-aligned silicon nanoparticles obtained by chemical deposition, reprinted with permission from Ref. 92. (b) Periodic Fe_2O_3 nanobeam-array with different periods fabricated via combination of lithography (top image) and oxidation in air (bottom), reprinted with permission from Ref. 93. (c) Dark-field optical image of silicon nanoparticles obtained by thin film dewetting, reprinted with permission from Ref. 87. (d) SiGe nanoparticles received after thermal dewetting, reprinted with permission from Ref. 90.

methods to fabricate functional structures.

The chemical procedures can be easily combined with lithography. In Ref. 93 the combination of lithography and oxidation in air was successfully implemented for the fabrication of a periodic Fe_2O_3 nanobeam-array for active photocatalytic material creation supporting optical Mie resonances, Fig. 6(b). Chemical methods can also be combined with standard commercial products to generate nanostructures for new dielectric metamaterial designs, e.g. SiC whiskers available commercially were washed in ethanol and studied [27].

Thus, chemical methods provide large opportunities for researchers. Whereas, inherent disadvantages (chemical waste, possible contamination of fabricated nanomaterials, additional steps for generation nanostructures, etc.) impose constraints on possible application areas.

Dewetting

Dewetting of a thin film is another process that can be applied for fabrication of high-index nanoparticles on a large scale. This process implies agglomeration of nanoparticles during heating of a thin film due to minimization of total energy of the thin film surfaces, including a film-substrate interface [105, 106]. The film thickness has a direct influence on the dewetting process (the lower the thickness, the higher the driving force for

dewetting) [106], therefore dewetting can be carried out at temperatures lower than the melting threshold of the thin film material. Overall, the main controlling parameters in this method are the heating temperature and properties of the thin film (thickness, presence of defects and initial patterns).

Dewetting has been applied for the fabrication of silicon nanoparticles with different sizes after heating of thin crystalline [87] or amorphous [88] silicon films. This method also enables a controlled formation of complex assemblies of silicon monocrystalline resonators, Fig. 6(c) [87]. It should be noted, that in the thin film dewetting technique the nanoparticle size and location control can be achieved only by using additional lithographic methods, which is even more complicated compared to the chemical deposition techniques.

In spite of this fact, dewetting offers great opportunities in terms of productivity and can be applied to any material. In Ref. 89 it was demonstrated, that the appropriate choice of the substrate temperature during the growth process provides an effective approach for the creation of needle-like Te crystallites. In Ref. 90, two-component SiGe nanoparticles were obtained after thermal dewetting. In this work thermal dewetting and agglomeration of the Ge layer deposited on a 9 nm thick Si (001) layer was investigated. It was demonstrated, that Ge layer lowers the dewetting temperature and makes it possible the creation of SiGe nanoparticles (see Fig. 6(d)).

Thereby, dewetting is simple and highly productive method for the fabrication of high-index nanoparticles. However, controllable arrangement of nanoparticles in certain places on the sample surface is still a problem for this method.

Laser-assisted methods

Fast progress in nanotechnologies demands growing precision of fabrication processes. It is not surprising, that laser-assisted methods are applied in different nanofabrication processes due to their material selectivity, submicron resolution, high energy density, etc. For example, laser-assisted methods were proven to be effective for the fabrication of nanoparticles with the diameters less than 100 nm. It is worth noting that colloids of chemically pure nanoparticles can be obtained by means of laser ablation in liquids. The main advantages of the ablation approach are relatively high productivity and lack of harmful chemical wastes.

The growing interest in the fabrication of high-index nanoparticles stimulated application of laser-assisted methods for the generation of nanoparticles with the sizes larger than 100 nm supporting Mie resonances in the visible and near-IR regions. Studies in this field have only recently begun and laser-assisted methods were applied

Laser-assisted methods

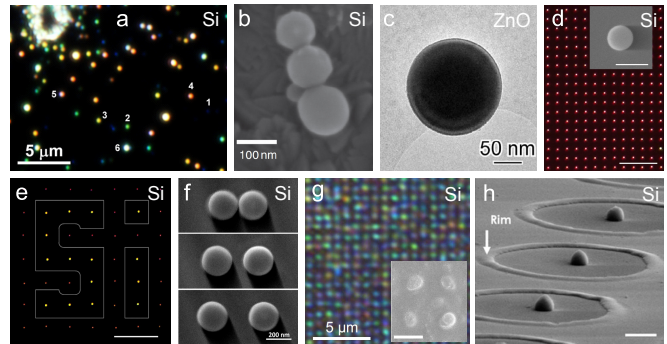


FIG. 7. (a) Dark-field optical image of silicon nanoparticles obtained via femtosecond laser ablation of bulk silicon, reprinted with permission from Ref. 21. (b) SEM image of a silicon nanosphere trimer, reprinted with permission from Ref. 107. (c) TEM image of a ZnO submicrosphere, reprinted with permission from Ref. 95. (d-e) Demonstration of the laser printing method: (d) Array of amorphous Si nanoparticles fabricated by LIT method and visualized with dark-field microscopy (scale bar, $20 \mu\text{m}$). The insert shows a SEM image of a single Si nanoparticle in this array (scale bar, 200 nm). (e) Dark-field optical image of silicon nanoparticles obtained via femtosecond laser ablation of thin silicon film. In picture (e) red nanoparticles are amorphized, while yellow are annealed and crystalline. Reprinted with permission from Ref. 22. (f) SEM-images of Si nanoparticle dimer structures on a glass substrate. Reprinted with permission from Ref. 75. (g) Optical image of an array of the silicon nanoparticles fabricated by direct laser writing, inset displays SEM image of the written nanoparticles covered by a 10 nm gold layer with the scale bar of 700 nm. Reprinted with permission from Ref. 108. (h) SEM pictures of silicon nanodome array produced by donut-shaped laser beam pulses. Reprinted with permission from Ref. 109.

mostly to silicon.

Ablation of bulk materials

First experiments towards fabrication of high-index nanoparticles using laser-assisted methods were conducted by direct laser ablation: an ultrashort laser pulse induced material fragmentation into spherical nanoparticles and their deposition close to the focus area, Fig. 7(a) [20, 21, 44, 94, 96]. Laser ablation in superfluid helium was also successfully implemented for the fabrication of single-crystalline sub- and micron-sized ZnO, CdSe, ZnSe, and CeO_2 microspheres, Fig. 7(b),(c) [95]. These experiments proved the effectiveness of laser ablation for the fabrication of high-index nanoparticles with optical response (scattering efficiencies, Q-factors, etc.) in the visible and IR spectral ranges. However, application of such processes in nanophotonics is a problem due to inability to control the fabricated nanoparticle sizes and their locations. To overcome these problems, other

laser-assisted methods were developed.

Laser-induced transfer

Laser-induced transfer (LIT) methods, demonstrated for the first time in the 80s [110], has become a promising approach for laser printing of nanoparticles from different materials: metals and semiconductors. In this method, laser radiation is focused on the interface between the printed material and transparent donor substrate providing material transfer onto another receiver substrate placed in a closed contact with the donor sample. First experiments on the fabrication of silicon nanoparticles with Mie-resonances in the visible range using laser printing were performed in Ref. 22. With this technique highly ordered arrays of nanoparticles can be produced [22], also dimers consisting of submicron crystalline silicon nanoparticles with different interparticle distances, ranging from 5 nm to 375 nm, have been demonstrated (Fig. 7(f) [75]). It should be mentioned that laser annealing can be applied for postprocessing of laser printed semiconductor nanoparticles to controllably change their phase from initially amorphous state to crystalline. This allows tailoring their optical properties, e.g., for silicon nanoparticles, Fig. 7(e) [22]. Therefore, laser printing technique is very attractive for the fabrication of high-index nanoparticles and their arrangement in 2D arrays with a high precision.

Laser-induced dewetting

Laser radiation can be applied for patterning of thin films of high-index materials by their controlled dewetting into nanoscale structures. In Ref. 108, crystalline silicon nanoparticles were fabricated from amorphous silicon films without applying initially crystalline materials or any additional annealing steps (Fig. 7(g)). Laser-based dewetting of amorphous silicon thin films by donut-shaped laser beams was demonstrated in Ref. 109, where morphological modification of the film into a nanodome (Fig. 7(h)) during thermocapillary-induced dewetting lead to phase transformation from amorphous to crystalline structure in the laser focus area. Thus, laser-assisted dewetting combining advantages of dewetting and direct laser patterning can be considered as a promising method for large scale fabrication of high-index nanoparticles.

To summarize, it should be noted that laser-assisted methods require high quality laser radiation (high laser pulse stability, perfect beam shape, and excellent focusing), including high precision and reliability of the position systems. However, these constrains do not lessen the basic advantages of the laser-assisted methods (single step process, high repeatability, modification of nanopar-

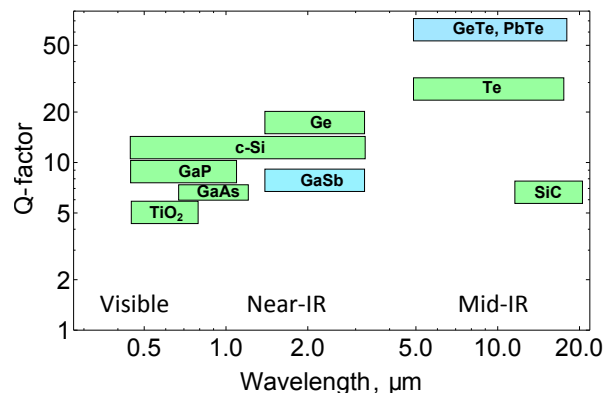


FIG. 8. High-refractive index materials for all-dielectric nanophotonics: Q -factors of spherical resonators made from these materials. Materials which can be nanostructured by the available fabrication techniques are marked by green, non-structurable materials are marked by blue color.

ticles crystalline phase, space arrangement of the fabricated nanoparticles), which all are important for the realization of nanophotonic devices.

DISCUSSION AND OUTLOOK

An overview of the available high-index materials and nanofabrication methods for their potential applications in all-dielectric nanophotonics has been given. Figure 8 briefly summarizes our analysis of high-refractive index materials. In this plot, materials for which nanoparticle fabrication methods have been demonstrated are highlighted by green color, while materials, for which nanofabrication has not been demonstrated so far, are highlighted by blue color. Optical performance of each material in terms of the resonance quality factor is determined by the trade-off between the refractive index and related optical absorption.

In the visible region, silicon nanoantennas provide highest field enhancement, while GaP may be preferable for the realization of metasurfaces due to smaller absorption. In the near-IR region, germanium is the best high-index material, while the narrow band-gap semiconductors, such as GeTe and PbTe, are more promising for the mid-IR range.

In terms of nanofabrication, currently developed approaches allow production of different types of all-dielectric functional structures with the desired optical properties. The development of hybrid nanostructures combining plasmonic and Mie resonances will be interesting for different applications in nanophotonics, medicine, ecology, etc.

Further research in this field can be devoted to the search for other materials demonstrating superior behavior in the visible and near-IR regions. Consideration of indirect band gap semiconductors, where optical absorp-

tion is suppressed due to the mismatch between photon and electron wavevectors, is promising. We think that the ideal high-index material could be found among narrow-gap indirect semiconductors.

It is also possible to use gapless direct semiconductors or semimetals, including 3D Dirac semimetals [111–113], where absorption is suppressed due to optical Pauli blocking. However, for applications in the visible range, one needs materials with very high Fermi level ($E_f > 1$ eV). Optical constants are not determined solely by the electronic band structure. They can be modified by phonon-polariton resonances. These resonances can give a higher refractive index simultaneously bringing losses. Large density of phonon modes at room temperature prevents currently known gapless semiconductors and 3D Dirac semimetals from becoming candidates for lossless high-index materials. On the other hand, specific fabrication techniques should be developed to explore potential of narrow band gap semiconductors, such as PbTe and GeTe, as materials for sub-wavelength mid-IR resonators.

We hope that the provided analysis will serve for better understanding of design rules of high-index nano-resonators and will facilitate the development of highly-efficient optical devices.

Authors acknowledge fruitful discussion with Philippe Tassin, Boris Luk'yanchuk, Andrea Alu, Pavel Belov, and Yuri Kivshar.

† These authors contributed equally to this manuscript.

* denisb@chalmers.se

- [1] M. Pelton, J. Aizpurua, and G. Bryant, *Laser Photon. Rev.* **2**, 136 (2008).
- [2] J. A. Schuller, E. S. Barnard, W. Cai, Y. C. Jun, J. S. White, and M. L. Brongersma, *Nat. Mater.* **9**, 193 (2010).
- [3] V. Giannini, A. I. Fernandez-Dominguez, S. C. Heck, and S. A. Maier, *Chemical Reviews* **111**, 3888 (2011).
- [4] X. Fan, W. Zheng, and D. J. Singh, *Light Sci. Appl.* **3**, e179 (2014).
- [5] P. R. West, S. Ishii, G. V. Naik, N. K. Emani, V. M. Shalaev, and A. Boltasseva, *Laser Photon. Rev.* **4**, 795 (2010).
- [6] J. B. Khurgin and G. Sun, *App. Phys. Lett.* **100**, 11105 (2012).
- [7] J. B. Khurgin, *Nat. Nanotechnol.* **10**, 2 (2015).
- [8] M. Gather, K. Meerholz, N. Danz, and K. Leosson, *Nature Photon.* **4**, 457 (2010).
- [9] S. Wuestner, A. Pusch, K. L. Tsakmakidis, J. M. Hamm, and O. Hess, *Phys. Rev. Lett.* **105**, 127401 (2010).
- [10] M. I. Stockman, *Phys. Rev. Lett.* **106**, 156802 (2011).
- [11] A. Pusch, S. Wuestner, J. M. Hamm, K. L. Tsakmakidis, O. Hess, M. A. Maxwell-bloch, A. Pusch, S. Wuestner, J. M. Hamm, K. L. Tsakmakidis, and O. Hess, *ACS Nano* **6**, 2420 (2012).
- [12] A. A. Lisyansky, I. A. Nechepurenko, A. V. Dorofeenko, A. P. Vinogradov, and A. A. Pukhov, *Phys. Rev. B* **84**, 153409 (2011).
- [13] E. S. Andrianov, D. G. Baranov, A. A. Pukhov, A. V. Dorofeenko, A. P. Vinogradov, and A. A. Lisyansky, *Opt. Express* **21**, 13467 (2013).
- [14] J. B. Khurgin and G. Sun, *Appl. Phys. Lett.* **96**, 181102 (2010).
- [15] G. V. Naik, V. M. Shalaev, and A. Boltasseva, *Adv. Mater.* **25**, 3264 (2013).
- [16] K. Feng, W. Streyer, Y. Zhong, A. Hoffman, and D. Wasserman, *Opt. Express* **23**, A1418 (2015).
- [17] G. Mie, *Ann. Phys. (Berlin)* **330**, 377 (1908).
- [18] R. Fenollosa, F. Meseguer, and M. Tymczenko, *Adv. Mater.* **20**, 95 (2008).
- [19] E. Xifre-Perez, R. Fenollosa, and F. Meseguer, *Opt. Express* **19**, 3455 (2011).
- [20] A. B. Evlyukhin, S. M. Novikov, U. Zywiets, R. L. Eriksen, C. Reinhardt, S. I. Bozhevolnyi, and B. N. Chichkov, *Nano Lett.* **12**, 3749 (2012).
- [21] A. I. Kuznetsov, A. E. Miroshnichenko, Y. H. Fu, J. Zhang, and B. Luk'yanchuk, *Sci. Rep.* **2**, 492 (2012).
- [22] U. Zywiets, A. B. Evlyukhin, C. Reinhardt, and B. N. Chichkov, *Nat. Commun.* **5**, 3402 (2014).
- [23] S. Jahani and Z. Jacob, *Nat. Nanotechnol.* **11**, 23 (2016).
- [24] A. I. Kuznetsov, A. E. Miroshnichenko, M. L. Brongersma, Y. S. Kivshar, and B. Lukyanchuk, *Science* **354**, aag2472 (2016).
- [25] M. S. Wheeler, J. S. Aitchison, and M. Mojahedi, *Phys. Rev. B* **72**, 193103 (2005).
- [26] B. I. Popa and S. A. Cummer, *Phys. Rev. Lett.* **100**, 1 (2008).
- [27] J. A. Schuller, R. Zia, T. Taubner, and M. L. Brongersma, *Phys. Rev. Lett.* **99**, 1 (2007).
- [28] J. C. Ginn, I. Brener, D. W. Peters, J. R. Wendt, J. O. Stevens, P. F. Hines, L. I. Basilio, L. K. Warne, J. F. Ihlefeld, P. G. Clem, and M. B. Sinclair, *Phys. Rev. Lett.* **108**, 097402 (2012).
- [29] A. B. Evlyukhin, C. Reinhardt, A. Seidel, B. S. Lukyanchuk, and B. N. Chichkov, *Phys. Rev. B* **82**, 45404 (2010).
- [30] P. Moitra, B. A. Slovick, W. Li, I. I. Kravchenko, D. P. Briggs, S. Krishnamurthy, and J. Valentine, *ACS Photonics* **2**, 692 (2015).
- [31] A. Arbabi, Y. Horie, M. Bagheri, and A. Faraon, *Nat. Nanotechnol.* **10**, 937 (2015).
- [32] M. I. Shalaev, J. Sun, A. Tsukernik, A. Pandey, K. Nikolskiy, and N. M. Litchinitser, *Nano Lett.* **15**, 6261 (2015).
- [33] M. Khorasaninejad, W. T. Chen, R. C. Devlin, J. Oh, A. Y. Zhu, and F. Capasso, *Science* **352**, 1190 (2015).
- [34] Y. F. Yu, A. Y. Zhu, R. Paniagua-Domínguez, Y. H. Fu, B. Luk'yanchuk, and A. I. Kuznetsov, *Laser Photon. Rev.* **9**, 412 (2015).
- [35] B. Rolly, B. Bebey, S. Bidault, B. Stout, and N. Bonod, *Phys. Rev. B* **85**, 245432 (2012).
- [36] P. Albella, M. A. Poyli, M. K. Schmidt, S. A. Maier, F. Moreno, J. J. Saenz, and J. Aizpurua, *J. Phys. Chem. C* **117**, 13573 (2013).
- [37] P. A. Dmitriev, D. G. Baranov, V. A. Milichko, S. V. Makarov, I. S. Mukhin, A. K. Samusev, A. E. Krasnok, P. A. Belov, and Y. S. Kivshar, *Nanoscale* **8**, 9721 (2016).

- [38] A. Krasnok, S. Glybovski, M. Petrov, S. Makarov, R. Savelev, P. Belov, C. Simovski, and Y. Kivshar, *Appl. Phys. Lett.* **108**, 211105 (2016).
- [39] A. E. Krasnok, A. E. Miroshnichenko, P. a. Belov, and Y. S. Kivshar, *Opt. Express* **20**, 20599 (2012).
- [40] A. García-Etxarri, R. Gómez-Medina, L. S. Froufe-Pérez, C. López, L. Chantada, F. Scheffold, J. Aizpurua, M. Nieto-Vesperinas, and J. J. Sáenz, *Opt. Express* **19**, 4815 (2011).
- [41] J. M. Geffrin, B. García-Cámara, R. Gómez-Medina, P. Albella, L. S. Froufe-Pérez, C. Eyraud, A. Litman, R. Vaillon, F. González, M. Nieto-Vesperinas, J. J. Sáenz, and F. Moreno, *Nat. Commun.* **3**, 1171 (2012).
- [42] A. B. Evlyukhin, R. L. Eriksen, W. Cheng, J. Beer-mann, C. Reinhardt, A. Petrov, S. Prorok, M. Eich, B. N. Chichkov, and S. I. Bozhevolnyi, *Sci. Rep.* **4**, 4126 (2014).
- [43] P. Albella, T. Shibanuma, and S. A. Maier, *Sci. Rep.* **5**, 18322 (2015).
- [44] Y. H. Fu, A. I. Kuznetsov, A. E. Miroshnichenko, Y. F. Yu, and B. Luk'yanchuk, *Nat. Commun.* **4**, 1527 (2013).
- [45] R. S. Savelev, S. V. Makarov, A. E. Krasnok, and P. A. Belov, *Opt. Spectrosc.* **119**, 551 (2015).
- [46] S. V. Li, D. G. Baranov, A. E. Krasnok, and P. A. Belov, *Appl. Phys. Lett.* **107**, 171101 (2015).
- [47] D. Markovich, K. Baryshnikova, A. Shalin, A. Samusev, A. Krasnok, and P. Belov, *Sci. Rep.* **6**, 22546 (2016).
- [48] M. R. Shcherbakov, D. N. Neshev, B. Hopkins, A. S. Shorokhov, I. Staude, E. V. Melik-Gaykazyan, M. Decker, A. A. Ezhov, A. E. Miroshnichenko, I. Brener, A. A. Fedyanin, and Y. S. Kivshar, *Nano Lett.* **14**, 6488 (2014).
- [49] S. Makarov, S. Kudryashov, I. Mukhin, A. Mozharov, V. Milichko, A. Krasnok, and P. Belov, *Nano Lett.* **15**, 6187 (2015).
- [50] M. R. Shcherbakov, P. P. Vabishchevich, A. S. Shorokhov, K. E. Chong, D.-Y. Choi, I. Staude, A. E. Miroshnichenko, D. N. Neshev, A. A. Fedyanin, and Y. S. Kivshar, *Nano Lett.* **15**, 6985 (2015).
- [51] D. G. Baranov, S. V. Makarov, V. A. Milichko, S. I. Kudryashov, A. E. Krasnok, and P. A. Belov, *ACS Photonics* **3**, 1546 (2016).
- [52] S. A. Maier, *Opt. Express* **14**, 1957 (2006).
- [53] P. Bharadwaj, B. Deutsch, and L. Novotny, *Adv. Opt. Photon.* **1**, 438 (2009).
- [54] M. Agio, *Nanoscale* **4**, 692 (2012).
- [55] T. J. Seok, A. Jamshidi, M. Kim, S. Dhuey, A. Lakhani, H. Choo, P. J. Schuck, S. Cabrini, A. M. Schwartzberg, J. Bokor, E. Yablonovitch, and M. C. Wu, *Nano Letters* **11**, 2606 (2011).
- [56] C. F. Klingshirm, *Semiconductor Optics* (Springer, 2012).
- [57] P. Y. Yu and M. Cardona, *Fundamentals of Semiconductors* (Springer, 2010).
- [58] H. M. Nussenzweig, *Causality and Dispersion Relations* (Academic Press, New York, 1972).
- [59] J. D. Caldwell, L. Lindsay, V. Giannini, I. Vurgaftman, T. L. Reinecke, S. A. Maier, and O. J. Glembocki, *Nanophotonics* **4**, 44 (2015).
- [60] M. A. Green and M. J. Keevers, *Prog. Photovoltaics Res. Appl.* **3**, 189 (1995).
- [61] H. Li, *J. Phys. Chem. Ref. Data* **9**, 561 (1980).
- [62] D. Pierce and W. Spicer, *Phys. Rev. B* **5**, 3017 (1972).
- [63] G. Jellison, *Opt. Mater.* **1**, 151 (1992).
- [64] D. Aspnes and A. Studna, *Phys. Rev. B* **27**, 985 (1983).
- [65] J. R. DeVore, *J. Opt. Soc. Am.* **41**, 416 (1951).
- [66] E. D. Palik, *Handbook of optical constants of solids* (Academic Press, 1998).
- [67] R. Ferrini, M. Patrini, and S. Franchi, *J. Appl. Phys.* **84**, 4517 (1998).
- [68] R. S. Caldwell and H. Fan, *Phys. Rev.* **114**, 664 (1959).
- [69] F. Weiting and Y. Yixun, *Infrared Phys.* **30**, 371 (1990).
- [70] C. Okoye, *J. Phys. Condens. Matter* **14**, 8625 (2002).
- [71] J. I. Larruquert, A. P. Pérez-Marín, S. García-Cortés, L. Rodríguez-de Marcos, J. A. Aznárez, and J. A. Méndez, *J. Opt. Soc. Am. A* **28**, 2340 (2011).
- [72] T. S. Moss, *Phys. Status Solidi B* **131**, 415 (1985).
- [73] N. Ravindra, P. Ganapathy, and J. Choi, *Infrared Phys. Technol.* **50**, 21 (2006).
- [74] P. Herve and L. Vandamme, *Infrared Phys. Technol.* **35**, 609 (1994).
- [75] U. Zywiets, M. Schmidt, A. Evlyukhin, C. Reinhardt, J. Aizpurua, and B. Chichkov, *ACS Photonics* **2**, 913 (2015).
- [76] S. Campione, S. Liu, L. I. Basilio, L. K. Warne, W. L. Langston, T. S. Luk, J. R. Wendt, J. L. Reno, G. A. Keeler, I. Brener, *et al.*, *ACS Photonics* **3**, 2362 (2016).
- [77] L. Shi, T. Tuzer, R. Fenollosa, and F. Meseguer, *Adv. Mater.* **24**, 5934 (2012).
- [78] M. van de Haar, J. van de Groep, B. Brenny, and A. Polman, *Opt. Express* **24**, 2047 (2016).
- [79] E.-K. Lee, J.-H. Song, K.-Y. Jeong, J.-H. Kang, H.-G. Park, and M.-K. Seo, *Sci. Rep.* **5**, 10400 (2015).
- [80] J. Feng, Q. Li, and S. Fan, *Opt. Lett.* **35**, 3904 (2010).
- [81] I. Staude, A. Miroshnichenko, M. Decker, N. Fofang, S. Liu, E. Gonzales, J. Dominguez, T. Luk, D. Neshev, I. Brener, and Y. Kivshar, *ACS Nano* **7**, 7824 (2013).
- [82] P. Spinelli, M. Verschuuren, and A. Polman, *Nat. Commun.* **3**, 692 (2012).
- [83] S. Person, M. Jain, Z. Lapin, J. J. Saenz, G. Wicks, and L. Novotny, *Nano Lett.* **13**, 1806 (2013).
- [84] S. Liu, J. F. Ihlefeld, J. Dominguez, E. F. Gonzales, J. E. Bower, D. B. Burckel, M. B. Sinclair, and I. Brener, *Appl. Phys. Lett.* **102**, 161905 (2013).
- [85] P. Spinelli, B. Macco, M. A. Verschuuren, W. Kessels, and A. Polman, *Appl. Phys. Lett.* **102**, 233902 (2013).
- [86] M. Decker and I. Staude, *J. Opt.* **18**, 103001 (2016).
- [87] M. Abbarchi, M. Naffouti, B. Vial, A. Benkouider, L. Lermusiaux, L. Favre, A. Ronda, S. Bidault, I. Berbezier, and N. Bonod, *ACS Nano* **8**, 11181 (2014).
- [88] M. Naffouti, T. David, A. Benkouider, L. Favre, A. Ronda, I. Berbezier, S. Bidault, N. Bonod, and M. Abbarchi, *Nanoscale* **8**, 2844 (2016).
- [89] E. Weidmann and J. Anderson, *Thin Solid Films* **7**, 265 (1971).
- [90] P. Zhang, B. Yang, P. Rugheimer, M. Roberts, D. Savage, F. Liu, and M. Lagally, *J. Phys. D: Appl. Phys.* **42**, 175309 (2009).
- [91] J. Proust, F. Bedu, S. Chenot, I. Soumahoro, I. Ozerov, B. Gallas, R. Abdeddaim, and N. Bonod, *Adv. Opt. Mater.* **3**, 1280 (2015).
- [92] L. Shi, J. Harris, R. Fenollosa, I. Rodriguez, X. Lu, B. Korgel, and F. Meseguer, *Nat. Commun.* **4**, 1904 (2013).
- [93] S. J. Kim, I. Thomann, J. Park, J.-H. Kang, A. P. Vasudev, and M. L. Brongersma, *Nano Lett.* **14**, 1446 (2014).
- [94] T. Lewi, P. P. Iyer, N. A. Butakov, A. A. Mikhailovsky,

- and J. A. Schuller, *Nano Lett.* **15**, 8188 (2015).
- [95] S. Okamoto, K. Inaba, T. Iida, H. Ishihara, S. Ichikawa, and M. Ashida, *Sci. Rep.* **4**, 5186 (2014).
- [96] U. Zywietz, C. Reinhardt, A. Evlyukhin, T. Birr, and B. Chichkov, *Appl. Phys. A* **114**, 45 (2014).
- [97] J. Fan and P. Chu, *Small* **6**, 2080 (2010).
- [98] K. Tamarov, L. Osminkina, S. Zinovyev, K. Maximova, J. Kargina, M. Gongalsky, Y. Ryabchikov, A. Al-Kattan, A. Sviridov, M. Sentis, A. Ivanov, V. Nikiforov, A. Kabashin, and V. Timoshenko, *Sci. Rep.* **4**, 7034 (2014).
- [99] P. Blandin, K. Maximova, M. Gongalsky, J. Sanchez-Royo, V. Chirvony, M. Sentis, V. Timoshenko, and A. Kabashin, *J. Mater. Chem. B* **1**, 2489 (2013).
- [100] L. Gu, D. Hall, Z. Qin, E. Anglin, J. Joo, D. Mooney, S. Howell, and M. Sailor, *Nat. Commun.* **4**, 2326 (2013).
- [101] R. Kormer, B. Butz, E. Spiecker, and W. Peukert, *Cryst. Growth Des.* **12**, 1330 (2012).
- [102] R. C. Devlin, M. Khorasaninejad, W. T. Chen, J. Oh, and F. Capasso, *Proceedings of the National Academy of Sciences* **113**, 10473 (2016).
- [103] P. Genevet, F. Capasso, F. Aieta, M. Khorasaninejad, and R. Devlin, *Optica* **4**, 139 (2017).
- [104] W. O'Mara, R. B. Herring, and L. P. Hunt, *Handbook of semiconductor silicon technology* (Noyes Publications, 1990).
- [105] J. Ye and C. Thompson, *Adv. Mater.* **23**, 1567 (2011).
- [106] C. V. Thompson, *Annu. Rev. Mater. Res.* **42**, 399 (2012).
- [107] J. Yan, P. Liu, Z. Lin, H. Wang, H. Chen, C. Wang, and G. Yang, *Nat. Commun.* **6**, 7042 (2015).
- [108] P. Dmitriev, S. Makarov, V. Milichko, I. Mukhin, A. Gudovskikh, A. Sitnikova, A. Samusev, A. Krasnok, and P. Belov, *Nanoscale* **8**, 5043 (2015).
- [109] J.-H. Yoo, J. In, C. Zheng, I. Sakellari, R. Raman, M. Matthews, S. Elhadj, and C. Grigoropoulos, *Nanotechnology* **26**, 165303 (2015).
- [110] J. Bohandy, B. Kim, F. Adrian, and A. Jette, *J. Appl. Phys.* **63**, 1158 (1988).
- [111] Q. D. Gibson, L. M. Schoop, L. Muechler, L. S. Xie, M. Hirschberger, N. P. Ong, R. Car, and R. J. Cava, *Phys. Rev. B* **91**, 205128 (2015).
- [112] T. Wehling, A. Black-Schaffer, and A. Balatsky, *Adv. Phys.* **63**, 1 (2014).
- [113] H. Weng, X. Dai, and Z. Fang, *J. Phys. Condens. Matter* **28**, 303001 (2016).